Indian J Phys (February 2013) 87(2):185–193
DOI 10.1007/s12648-012-0215-y

ORIGINAL PAPER

Multi-component Erlang distribution of final-state particles produced in high energy collisions

E Q Wang[1], H R Wei[1], M A Rahim[2], S Fakhraddin[2] and F H Liu[1]*

[1]Institute of Theoretical Physics, Shanxi University, Taiyuan 030006, Shanxi, China

[2]Physics Department, Faculty of Science, Sana'a University, Sana'a, Republic of Yemen

Received: 08 August 2012 / Accepted: 11 October 2012 / Published online: 21 November 2012

Abstract: A unified formula on multiplicity distributions of final-state particles is studied in this paper to describe a variety of experimental data including multiplicity, mass, transverse mass, excitation energy, transverse energy, and transverse momentum distributions. It is assumed that the sources of final-state particles are subjected to the multi-source thermal model and the contributions of sources meet the Erlang distribution. Further the validity of the unified formula in descriptions of different distributions is tested. Experimental data of proton-antiproton ($p\overline{p}$), positron–proton ($e^{+}p$), electron-proton ($e^{-}p$), and nucleus-nucleus (AA) collisions are analyzed and found that the distributions of mentioned quantities can be described by the multi-component Erlang distribution.

Keywords: Multi-component Erlang distribution; Final-state particles; High energy collisions

PACS Nos.: 12.40.Ee; 24.60.-k; 25.40.-h

1. Introduction

Intermediate and high energy collisions have become indispensable parts of modern science and technology. The investigation of nuclear collisions at high energy is one of the major research topics in the modern nuclear physics. This investigation offers unique possibility to understand many significant problems, such as the internal structure of particles, the mechanism of collision process, the elementary particles in compound matter, and so on.

Recently, the energy of nuclear collisions at the LHC has already reached at a few TeV/nucleon which is higher than the maximum energy (0.98 + 0.98 TeV) at Fermilab, and is much higher than the Dubna energy (a few GeV/nucleon), the GSI energy (1–2 GeV/nucleon or 1–2 A GeV), the maximum SPS energy (200 A GeV), and the maximum RHIC energy (100 + 100 A GeV). More and more researchers concern the high energy collisions due to some new interesting phenomena. Many theoretical models, such as the Statistical Multifragmentation Model (SMFM) [1], the Expanding and Emitting Source Model [2] or the Expanding-Evaporating Source Model (ESS) [3], the Relativistic or Ultrarelativistic Quantum Molecular Dynamics Model (RQMD or UrQMD) [4–7], etc., are proposed. Some models have been introduced and based on different considerations of the course of nuclear collisions, some models [8–10] are mainly proposed and focused on the dynamical mechanism, and others [11–14] concern the theory of statistical physics. A great number of experimental data are analyzed using these and other models. In particular, the distributions of final-state particles play a critical role in the field of high energy collisions.

In experiments, some collaborations have reported new and detailed experimental results [15–22]. In this paper, we hope to use a unified formula to describe some different experimental data in a wide energy range from GeV to TeV. Experimental data of nucleus-nucleus (AA) collisions, including the data of C+C collisions measured by the spectrometer at GSI at 1–2 A GeV [15] and the result of interactions of 8.8 GeV ^{4}He with U and Bi nuclei using the Makrofol polycarbonate track detector [16], will be studied in the present work. Meanwhile, experimental data of proton-antiproton ($p\overline{p}$) [17], positron–proton ($e^{+}p$) [18], and electron-proton ($e^{-}p$) [18] collisions at high energies will be also analyzed. The data of $p\overline{p}$ collisions are

*Corresponding author, E-mail: fuhuliu@163.com

collected with the detector at the Fermilab Tevatron at center-of-mass energy of $\sqrt{s} = 1.96$ TeV [17]. And for the e^+p and e^-p collisions, the beam energies for positron, electron, and proton are 27.6, 27.6, and 920 GeV, respectively, corresponding to center-of-mass energy of 319 GeV [18]. In a few TeV energy range [19, 22], some of the data at the LHC are already analyzed [23, 24]. In this paper, to avoid repeating representation, we shall not analyze the data at the LHC energies.

2. The model

Now a days, various models are proposed to describe phenomena of collisions based on different methods. It is expected that a unified method is needed to explain more experimental data. Recently, a multi-source thermal model [25–29] is proposed and a unified formula (a multi-component Erlang distribution) is obtained [27–29]. A few experimental distributions are described by the unified formula [23, 24, 27–30]. To test further the validity of the unified formula, in the following discussions we introduce briefly the formula and explain more experimental data using it.

Generally, when a hard parton in projectile passing through hot and dense quantum chromodynamics (QCD) medium in target, it loses energy via medium induced gluon emission. The medium effect could modify the parton fragmentation process. In the center-of-mass reference frame the projectile and target have a symmetry property. The so-called "energy sources", i.e. partons, nucleons and nucleon clusters, in the framework of the multi-source thermal model obtain gluons with different energies. Many energy sources producing particles and fragments are expected to form in intermediate and high energy collisions. We would like to divide the sources into l groups according to the different impact parameters (participant nucleon numbers) or the different reaction mechanisms such as spallation, multi-fragmentation, evaporation, absorbtion, etc. The ith source in the jth group is assumed to obtain gluon energy. The probability distribution of gluon energy obtained by the source obeys an exponential function. The source number in the jth group and the weight of the jth group are denoted by m_j and k_j respectively.

As it was done in our recent work [30], in the case of considering different (X) distributions, we have the contribution of the ith source in the jth group to be

$$f_{ij}(X_{ij}) = \frac{1}{\langle X_{ij}\rangle} \exp\left(-\frac{X_{ij}}{\langle X_{ij}\rangle}\right), \tag{1}$$

where $\langle X_{ij}\rangle$ denotes the mean X_{ij} contributed by the ith source in the jth group. The X distribution of the concerned particles contributed by the jth group is obtained to be an Erlang distribution

$$f_j(X) = \frac{X^{m_j-1}}{(m_j-1)!\langle X_{ij}\rangle^{m_j}} \exp\left(-\frac{X}{\langle X_{ij}\rangle}\right) \tag{2}$$

when the different sources in the jth group offer the same contribution. Then, the X distribution contributed by all the groups is given by a multi-component Erlang distribution

$$f(X) = \frac{1}{N}\frac{dN}{dX} = \sum_{j=1}^{l} k_j f_j(X). \tag{3}$$

Some physical quantities, such as multiplicity (n), mass (M), transverse mass (M_T), excitation energy (E^*), transverse energy (E_T), and transverse momentum (P_T) are regarded as X in the present work to give a further test of the multi-component Erlang distribution [23, 24, 27–30]. All calculations are performed by the Monte Carlo method.

3. Comparisons with experimental data

Figure 1 presents the multiplicity distributions of final-state $\pi^{\pm}$ produced in AA collisions (Fig. 1(a) and 1(b)) and jets produced in $p\overline{p}$ collisions [Fig. 1(c)] at high energies. The experimental data points for $\pi^{\pm}$ shown in Fig. 1(a) and 1(b) given in terms of $(1/N)\mathrm{d}N/\mathrm{d}n$ versus n are taken from the C+C collisions at incident beam energies of 1 A and 2 A GeV respectively [15] using the High Acceptance Di-Electron Spectrometer (HADES) [15, 31] at GSI, where N and n denote the number of events and multiplicity respectively. In the calculation for the two curves, there is only one group of sources. The group contains three sources and the mean multiplicity is 1.13 and 1.25 respectively. Comparing with the C+C collisions, we also exhibit the multiplicity distribution (data points in terms of events vs n) of jets observed from $p\overline{p}$ collisions at a center-of-mass energy of $\sqrt{s} = 1.96$ TeV [17] collected with the Collider Detector at Fermilab (CDF II) [17, 31] at the Fermilab Tevatron. In the calculation for the curve, we also have three sources forming a group, and take $\langle X_{i1}\rangle$ to be 0.70. The values of $\langle X_{i1}\rangle$ and m_1 obtained by fitting the experimental data are given in Table 1 with the χ^2 per degree of freedom (χ^2/dof). One can see that the experimental distributions of the numbers of final-state particles and jets are in reasonable agreement with the results of the model.

Figures 2 and 3 show respectively the mass and transverse mass distributions of final-state particles produced in $p\overline{p}$ collisions at $\sqrt{s} = 1.96$ TeV and $e^{\pm}p$ collisions at $\sqrt{s} = 319$ GeV. The points in Figs. 2, 3(a) and 3 (b) represent the experimental data [17] collected by the CDF II detector from $p\overline{p}$ collisions [17, 32–35], and those in Fig. 3(c) are measured by the H1 [36] and ZEUS [18, 37] Collaborations at the HERA from the e^+p and e^-p collisions. In Fig. 2, the

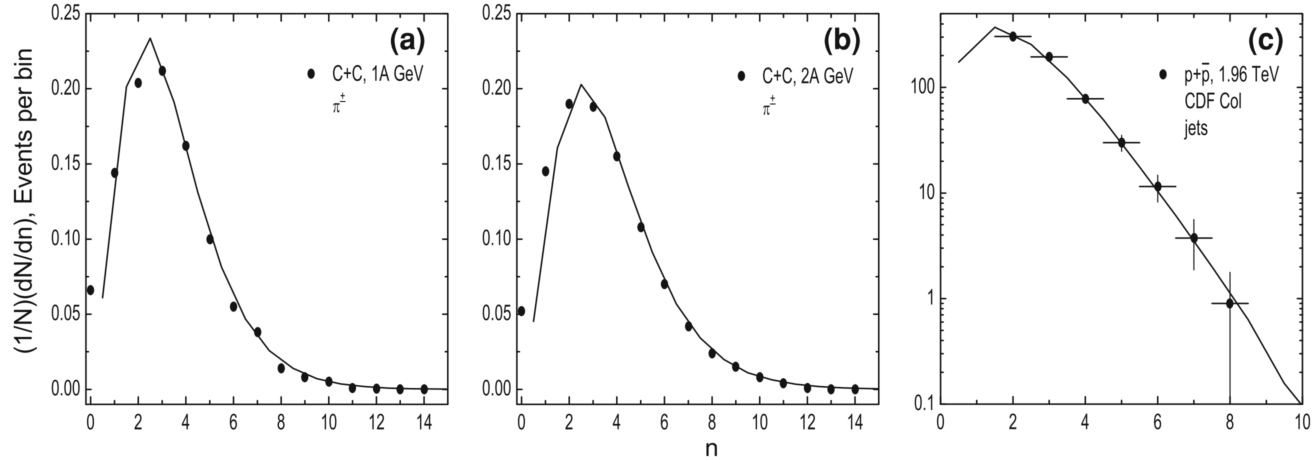

Fig. 1 Multiplicity distributions of final-state $\pi^{\pm}$ measured in C+C collisions at (**a**) 1 A GeV and (**b**) 2 A GeV, as well as (**c**) jets observed in $p\bar{p}$ collisions at $\sqrt{s} = 1.96$ TeV. The points represent the experimental data quoted in [15] in terms of $(1/N)\mathrm{d}N/\mathrm{d}n$ versus n (a, b) and [17] in terms of events versus n (c) respectively. The curves are our calculated results. For (**a**), (**b**), and (**c**), the normalization constants are 1, 1, and number of events, respectively

Table 1 Values of $\langle X_{ij}\rangle, m_j, k_j$, and χ^2/dof corresponding to the fits in Figs. 1–6

Figures	$\langle X_{i1}\rangle$	m_1	k_1	$\langle X_{i2}\rangle$	m_2	k_2	$\langle X_{i3}\rangle$	m_3	χ^2/dof
1(a)	1.13	3	1						0.392[a]
1(b)	1.25	3	1						1.260[a]
1(c)	0.70	3	1						0.261
2(a)	0.185	5	0.758	0.240	7	0.242			1.512[a]
2(b)	0.2	4	0.833	0.5	6	0.167			0.286
2(c)	19.0	5	0.909	20.0	12	0.091			0.240
2(d)	21.3	6	0.741	34.0	8	0.259			0.715
2(e)	33.0	3	1						0.472
3(a)	2.4	23	0.474	8.0	3	0.197	8.0	12	1.080
3(b)	22.0	5	1						1.783[b]
3(c)	4.3	12	1						0.864[c]
4(a)	0.560	4	1						0.266[c]
4(b)	0.640	6	1						0.326[c]
4(c)	0.435	6	1						0.435[c]
4(d)	0.580	6	1						0.360[c]
5(a)	30.0	1	0.926	28.0	6	0.074			0.337
5(b)	18.0	2	0.860	28.0	5	0.140			0.309
5(c)	17.0	11	0.750	30.0	13	0.250			0.707[b]
5(d)	3.37	3	0.998	7.50	6	0.002			0.298[b]
5(e)	44.0	1	1						0.314
6(a)	8.0	4	0.600	4.5	2	0.400			0.682[b]
6(b)	7.5	4	0.432	5.0	1	0.568			0.493
6(c)	3.9	9	1						0.308[b]
6(d)	4.5	9	1						0.374[b]
6(e)	22.0	1	1						0.683
6(f)	21.0	1	1						0.299

[a] We estimate the relative errors of the experiment data being 5 %

[b] The last point is not included in the calculation of χ^2/dof

[c] The first point is not included in the calculation of χ^2/dof

secondary vertex (SV) masses are fitted in events containing standard photons for (a) the control sample (CS) and (b) the search sample (SS) respectively, where the standard photons are photon candidates which are required to have no associated track with transverse momentum $P_T > 1$ GeV/c and at most one track with $P_T < 1$ GeV/c pointing at the calorimeter cluster, good profiles of electromagnetic energy measured in both transverse dimensions at the shower maximum and minimal leakage into the hadron calorimeter, and the ratio of hadronic energy to electromagnetic energy $E_{\mathrm{had}}/E_{\mathrm{em}}$ must be less than $0.055 + 0.00045\ E_{\mathrm{em}}$ (GeV). The CS is the photon + b-tag sample in which the only selection requirements are that there be at least one photon with pseudorapidity $|\eta| < 1.1$ and transverse energy $E_T < 25$ GeV and one SV-tagged jet having $|\eta| < 2$ and $E_T > 15$ GeV. The SS is the photon + b events obtained by subtracting the misidentified photon plus b contribution from the CS and then multiplying by an efficiency of 0.0123 ± 0.0025 which is derived from the fraction of the photon + b Monte Carlo simulation events in the CS [17]. The distributions of the masses of (c) the photon + b-quark jet ($\gamma + b$), (d) the b-quark jet + 2nd jet (untagged jet) (b + jet), and (e) the photon + b-quark jet + 2nd jet ($\gamma + b$ + jet) are given respectively in Fig. 2, too. In Fig. 3, the distributions of the transverse masses of (a) the photon + missing transverse energy ($\gamma + E_T^{\mathrm{miss}}$), (b) the b-quark jet + 2nd jet + missing transverse energy (b + jet + E_T^{miss}) and (c) the lepton-neutrino ($l + \nu$) are given, where the lepton-neutrino transverse mass is calculated using the vectors of the missing transverse momentum and the isolated lepton [18]. In the calculation for the curves, the values of $\langle X_{ij}\rangle, m_j, k_j$, and χ^2/dof are given in Table 1, where $\langle X_{ij}\rangle$ denotes $\langle M_{ij}\rangle$ or $\langle M_{Tij}\rangle$ in units of GeV/c^2. We see that the model describes the experimental data under consideration.

The distributions of excitation energies for events with different multiplicities $M_{\mathrm{IMF}}^{\mathrm{obs}}$ in AA collisions are given in Fig. 4, where $M_{\mathrm{IMF}}^{\mathrm{obs}}$ varying from 0 to 3 denotes the observed multiplicity of intermediate mass fragments. The points represent the experimental data in the interactions of 8.8 GeV ^{4}He with U and Bi nuclei examined using the Makrofol polycarbonate track detector [16]. The curves are our calculated results with $l = 1$ and different $\langle X_{i1}\rangle$ and m_1 presented in Table 1 with χ^2/dof, where $\langle X_{i1}\rangle$ is in units of GeV. One can see that the results calculated by the model are in agreement with the experimental data.

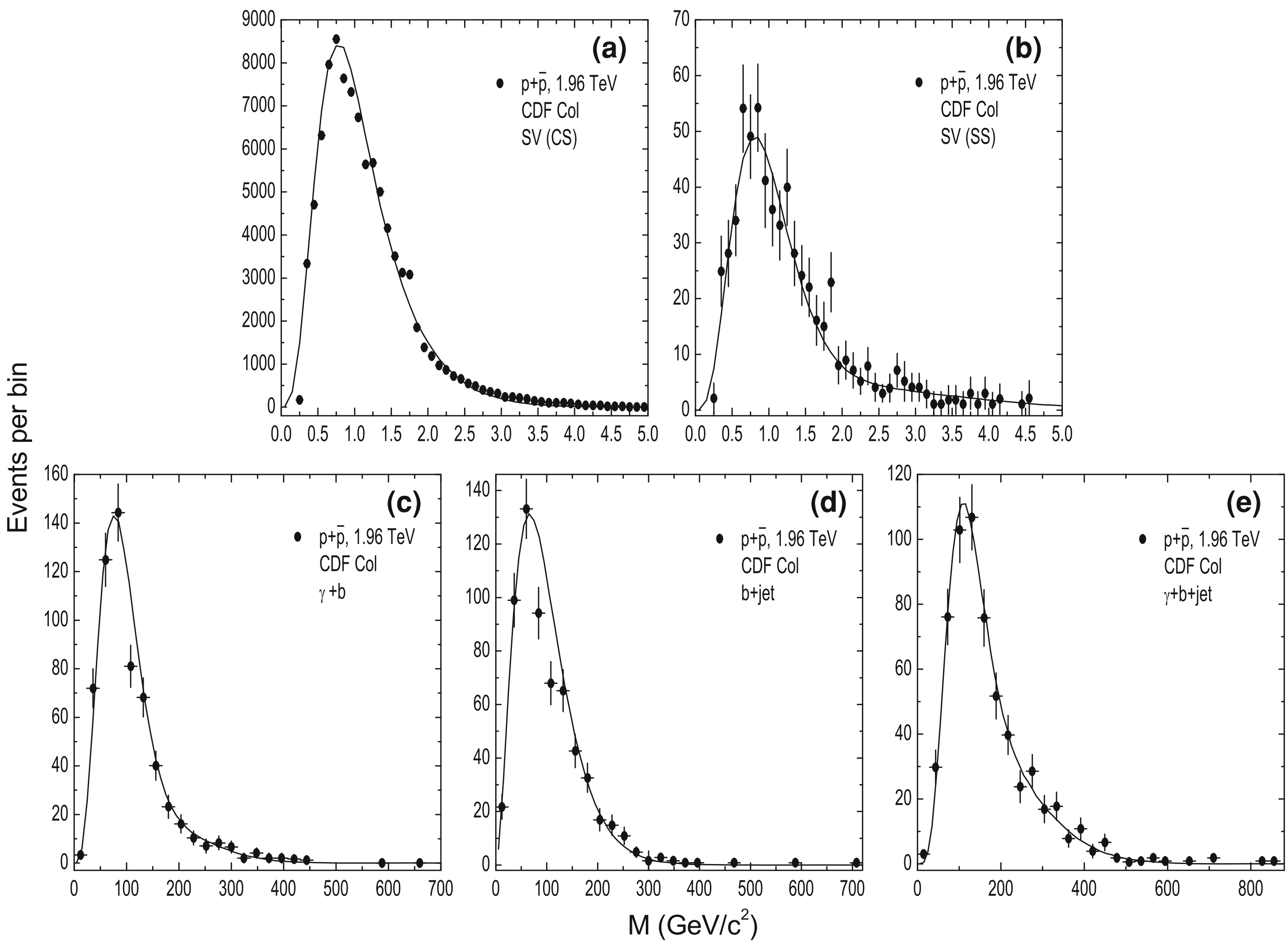

Fig. 2 Same as in Fig. 1, showing the mass distributions of final-state particles produced in $p\bar{p}$ collisions at $\sqrt{s} = 1.96$ TeV. The points represent the experimental data quoted in [17]. The secondary vertex (SV) masses are fitted in events containing standard photons for (**a**) the control sample (CS) and (**b**) the search sample (SS). The distributions of the masses of (**c**) the photon + b-quark jet ($\gamma + b$), (**d**) the b-quark jet + 2nd jet (untagged jet) (b + jet) and (**e**) the photon + b-quark jet + 2nd jet ($\gamma + b$ + jet) are given. The curves are the model fits using the multi-component Erlang distribution

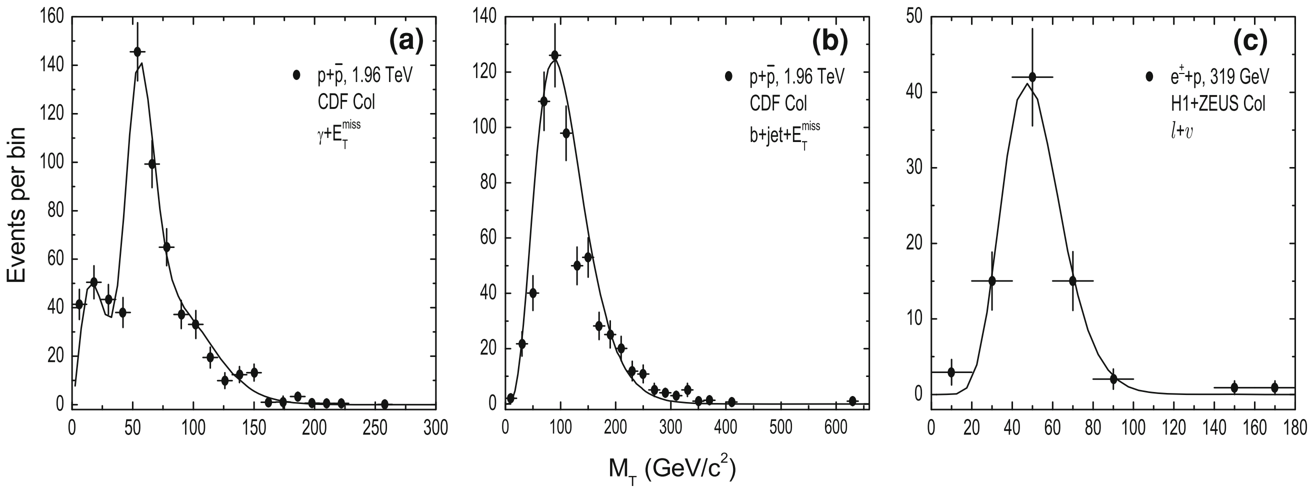

Fig. 3 Same as in Fig. 1, showing the transverse mass distributions of final-state particles produced in $p\bar{p}$ collisions at $\sqrt{s} = 1.96$ TeV (a,b) and $e^{\pm}p$ collisions at $\sqrt{s} = 319$ GeV (c). The points represent the experimental data quoted in [17] (**a**), (**b**) and [18] (**c**). The distributions of the transverse masses of (**a**) the photon + missing transverse energy ($\gamma + E_T^{\mathrm{miss}}$), (**b**) the b-quark jet + 2nd jet + missing transverse energy (b + jet + E_T^{miss}), and (**c**) the lepton-neutrino ($l + \nu$) are given, where the lepton-neutrino transverse mass is calculated using the vectors of the missing transverse momentum and the isolated lepton [18]. The curves are the model fits using the multi-component Erlang distribution

Figure 5 shows the transverse energy distributions of final-state particles produced in $p\bar{p}$ collisions at $\sqrt{s} = 1.96$ TeV. The points represent the experimental data collected by the CDF II detector [17] and the curves are our calculated results. The distributions in (a) the photon E_T, (b) the b-jet E_T, (c) the 2nd jet E_T, (d) the missing transverse energy E_T^{miss} and (e) the scalar sum of the transverse momenta of the γ, jets, and E_T^{miss} are displayed. The corresponding parameter values fitted by us are given in Table 1, and $\langle X_{ij}\rangle$ is in units of GeV. Once more the results calculated by the model are in agreement with the experiment data.

Figure 6(a)–(e) give the transverse momentum distributions (Events vs P_T) for different selected quantities in events with an isolated electron or muon and missing transverse momentum in the $e^{\pm}p$, $e^{+}p$, and $e^{-}p$ collisions at $\sqrt{s} = 319$ GeV, as well as Fig. 6(f) the single W production cross section ($d\sigma_W/dP_T$) as a function of the hadronic transverse momentum in the $e^{\pm}p$ collisions at $\sqrt{s} = 317$ GeV. From Fig. 6(a)–(e), the selected quantities correspond to the hadronic (X) transverse momentum, the missing transverse momentum (P_T^{miss}), the transverse momentum of the lepton (l), the hadronic (X) transverse momentum in $e^{+}p$ collisions only, and the hadronic (X) transverse momentum in $e^{-}p$ collisions only, respectively. Different selected quantities correspond to different integrated luminosities as shown in the figure. The points represent a combined data analysis [18] of the H1 and ZEUS Collaborations [36, 37] and the curves are our calculated results. The corresponding values of $\langle X_{ij}\rangle, m_j, k_j$, and χ^2/dof are given in Table 1, where $\langle X_{ij}\rangle$ is in units of GeV/c. We see that the results calculated by the model are in agreement with the experimental data.

From Figs. 1–6 we see that the distributions of quantities including multiplicities, masses, transverse masses, excitation energies, transverse energies, and transverse momenta are selected for this study to give a wider and further test of the multi-component Erlang distribution. Some special selection requirements are presented due to the reason of the experimental data sample given in the related references. From Table 1 we see that the χ^2/dof are much smaller than 1 in most cases, which raises the concern that the model over-describes the data. This seems to show that there are too many parameters in the model. In fact, except a few cases, the free parameter numbers in most cases are only 2. Another probability leaded to smaller χ^2/dof is the large errors in the experimental data. This is indeed the situation of a few figure panels.

4. Discussion

We see from the above figures that the results calculated by the model are consistent with the quoted experimental data. In the multiplicity distributions, our results calculated by assuming three sources in only one group are in good agreement with the experimental yields. The mass and transverse mass distributions, as compared to the multiplicity distributions, are also satisfied to the multi-component Erlang distribution. But some of our calculated curves

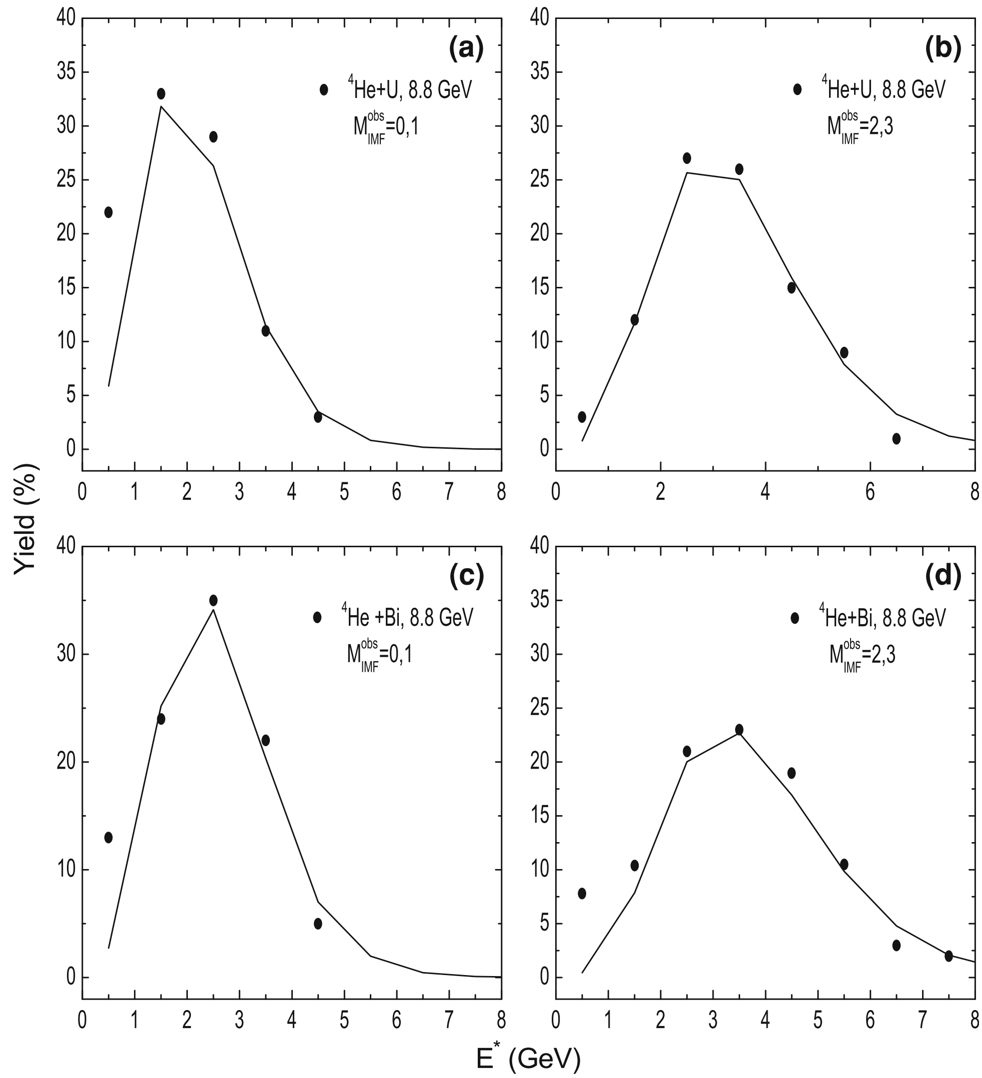

Fig. 4 Same as in Fig. 1, showing the excitation energy distributions for events with $M_{\rm IMF}^{\rm obs} = 0{,}1$ (**a**), (**c**) and $M_{\rm IMF}^{\rm obs} = 2{,}3$ (**b**), (**d**) in 8.8 GeV ^{4}He + U and Bi reactions. The points represent the experimental data quoted in [16]. The curves are the model fits using the multi-component Erlang distribution

are more precise to meet the experimental data by assuming two or three groups. We see also that the calculated excitation energy and transverse energy distributions by the multi-component Erlang distribution are in agreement with the available experimental data. The calculated distributions of transverse momenta by the formula are consistent with the experimental data, too.

In most cases, the group number is 1 or 2, and the source number in a given group is not too large. Generally, we regard partons or quarks and gluons as the energy sources. Especially, the energy sources contributed to final-state mesons are partons or quarks and gluons. For nuclear fragments the energy sources could be nucleons or nucleon clusters. Different distributions of multiplicities, masses, transverse masses, excitation energies, transverse energies, and transverse momenta described by a unified formula render that the energy sources contributed to the mentioned qualities are the same or similar. We think that these sources are mostly partons or quarks and gluons. The same or similar sources lead to the unified formula for different distributions.

It is difficult to predict the parameter values in this paper due to the limited data analysis on a given quantity. If we analyze the distributions of a given quantity at different conditions, we should obtain the dependence of parameter values on some factors [27–29]. Recently, the multi-component Erlang distribution is successfully used in the analyses of event-by-event fluctuations in nucleus-nucleus collisions at the SPS and the RHIC energies [30] and multiplicity distributions of charged particles in proton-proton collision at the LHC energies [23]. Considering different weights of different impact parameters or participant nucleon numbers, the multiplicity distributions in nucleus-nucleus collisions at GeV and TeV energies can be described by the model [24]. In fact, the multi-component Erlang distribution satisfies a wide energy range from GeV to TeV.

The multi-component Erlang distribution, which is widely used in the fields of stochastic processes is applied

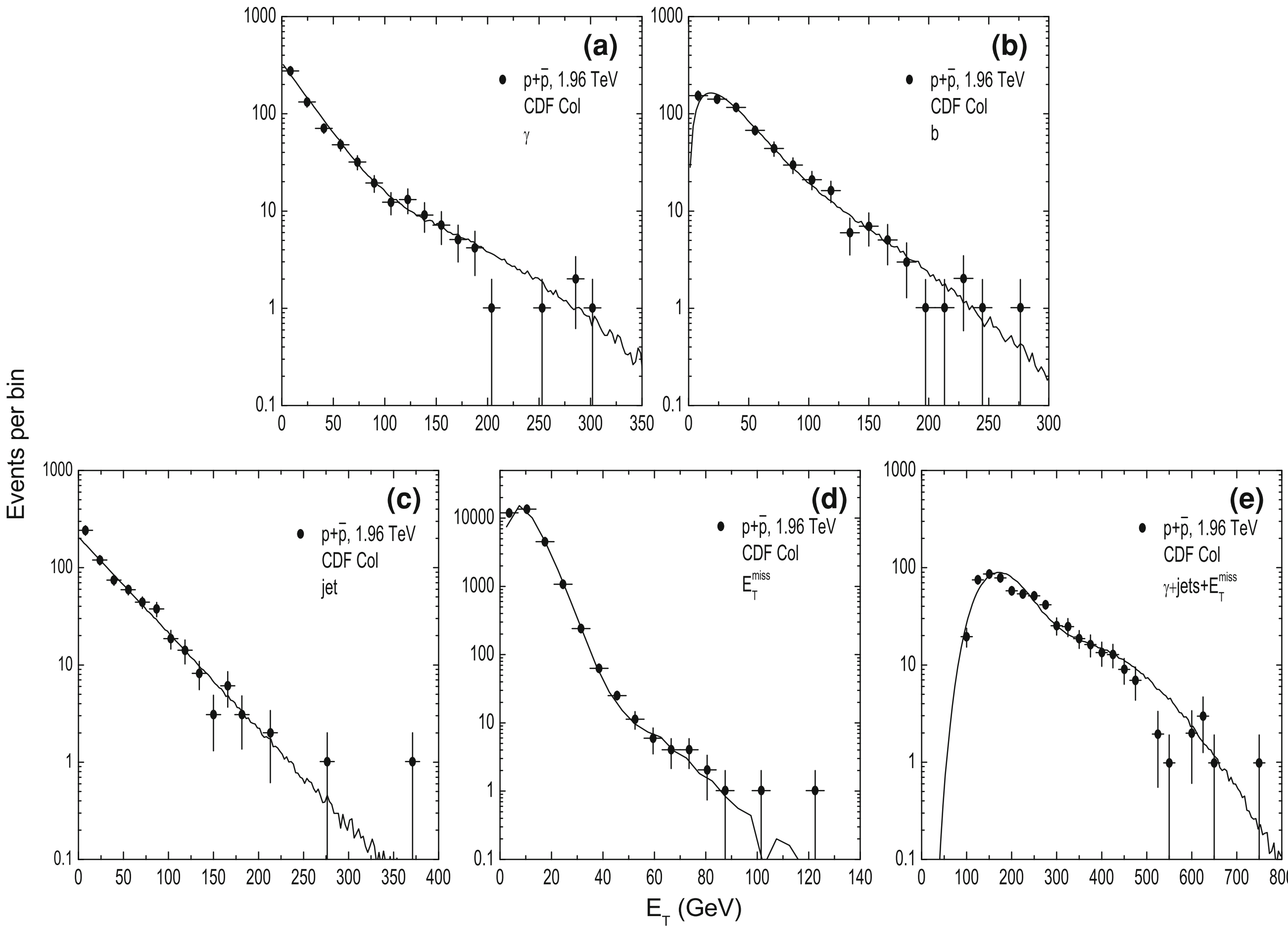

Fig. 5 Same as in Fig. 1, showing the transverse energy distributions of final-state particles produced in $p\bar{p}$ collisions at $\sqrt{s} = 1.96$ TeV. The points represent the experimental data quoted in [17]. The distributions in (**a**) the photon E_T, (**b**) the b-jet E_T, (**c**) the 2nd jet E_T, (**d**) the missing transverse energy E_T^{miss} and (**e**) the scalar sum of the transverse momenta of the γ, jets, and E_T^{miss} are displayed. The curves are the model fits using the multi-component Erlang distribution

by us to many physical quantities of produced particles in high energy collisions. Although we have published papers [27–30] analyzing different data from different collision systems and different energies with this model, the present work is applied to more data obtained at different systems and energies arguing the generality of the adopted approach. The multi-component Erlang distribution is indeed a common law in high energy collisions. Many physical quantities in the fields obey this law. Especially, in the case of component number being 1, the product $m_1 \langle X_{i1} \rangle$ determines the peak position of the distribution. A smaller m_1 and a larger $\langle X_{i1} \rangle$ give a wide distribution, and the reverse case gives a narrow distribution. A Gaussian-like distribution can be obtained by a larger m_1.

We notice that the multi-component Erlang distribution can not describe the rapidity (or pseudorapidity) distributions of charged particles produced in high energy collisions. As a longitudinal addition quantity in the Lorentz transformation, for a given parton energy loss in collisions, the rapidity is mainly determined by the incident energy. However, the quantities described by the multi-component Erlang distribution are mainly determined by the parton energy loss, or the energy obtained by the source, or the excited degree of the source. If the incident energies are different and the parton energy losses are the same, the multiplicity distribution should be the same and the rapidity distributions should be different. In other words, the multi-component Erlang distribution do describe the distributions of quantities related to the parton energy loss in collisions, and do not describe the distributions of quantities related to the energy carried out by the incident projectile. Generally, a large parton energy loss results a high excitation of the source and a wide probability distribution. We may say that, as a probability distribution, the multi-component Erlang distribution reflects a common law existed in energy loss phenomenon.

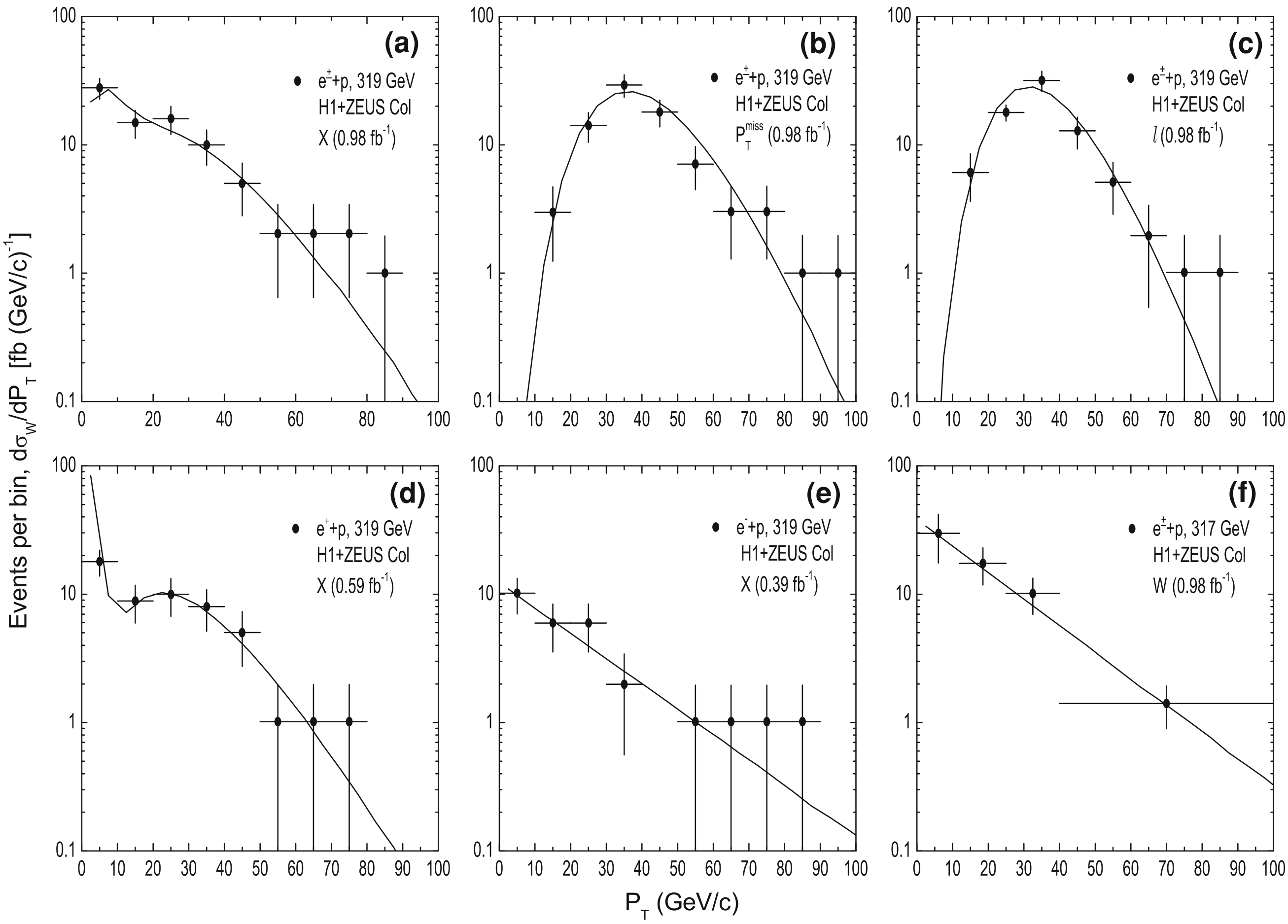

Fig. 6 Same as in Fig. 1, showing the transverse momentum distributions (Events vs P_T) (**a**)–(**e**) and the single W production cross section ($d\sigma_W/dP_T$) (**f**) for different selected quantities in e^+p and e^-p collisions at $\sqrt{s} = 319$ (**a**)–(**e**) and 317 (**f**) GeV. The points represent the experimental data quoted in [18]. From (**a**)–(**e**), the selected quantities correspond to the hadronic (X) transverse momentum, the missing transverse momentum ($P_T^{\rm miss}$), the transverse momentum of the lepton (l), the hadronic (X) transverse momentum in e^+p collisions only and the hadronic (X) transverse momentum in e^-p collisions only, respectively. Different selected quantities correspond to different integrated luminosities as shown in the figure. The curves are the model fits using the multi-component Erlang distribution

The multi-component Erlang distribution is a flexible representation on many distributions from the field of high energy particle and nuclear collisions. These distributions seem to concern various unrelated quantities, but all of the distributions have the features from exponential to Gaussian and their various superpositions. The multi-component Erlang distribution is in fact a simple superposition of Erlang functions. One component with $m_1 = 1$ gives an exponential distribution, and a large m_1 (above 10) gives the Gaussian-like distribution. From 1 to the large value, different values of m_1 show different distributions from exponential to Gaussian. Multiple components with different m_j can represent the distributions with abundant structures. Intermediate and high energy collisions are a complex process in which a lot of experimental data are obtained [38–42] and analyzed [43, 44]. As a primary analysis on common law, the present work is a wider and successful attempt. More meticulous and painstaking work which contains dynamical mechanisms is needed.

5. Conclusions

We have used a unified formula which is obtained in the framework of the multi-source thermal model to describe multiplicity, mass, transverse mass, transverse energy, and transverse momentum distributions of final-state particles in $p\overline{p}$ and $e^{\pm}p$ collisions, as well as excitation energy distribution for selected events in AA collisions at high energies. In the model, many energy sources are assumed to form in collisions. According to different interacting mechanisms or impact parameters, these sources are divided into l groups. The contribution of the ith source in the jth group is an exponential function. As a folding result of many exponential functions, an Erlang distribution can be obtained. The unified formula used by us is in fact a multi-component Erlang distribution. By using the formula, the mentioned distributions are described in the present work.

Acknowledgments This work was supported by the National Natural Science Foundation of China (10975095), the National Fundamental Fund of Personnel Training (J1103210), the Open Research Subject of the Chinese Academy of Sciences Large-Scale Scientific Facility (2060205), the Shanxi Provincial Innovative Foundation for Graduate Education (20123006) and the Shanxi Scholarship Council of China.

References

[1] J P Bondorf et al. *Phys. Rep.* **257** 133 (1995)
[2] W A Friedman *Phys. Rev. Lett.* **60** 2125 (1988)
[3] W A Friedman *Phys. Rev.* **C42** 667 (1990)
[4] J Aichelin et al. *Phys. Rev.* **C37** 2451 (1988)
[5] G Peilert, H Stöcker and W Greiner *Phys. Rev.* **C39** 1402 (1989)
[6] S A Bass et al. *Prog. Part. Nucl. Phys.* **41** 225 (1998)
[7] M. Bleicher et al. *J. Phys.* **G25** 1859 (1999)
[8] G F Bertsch and H Kruse *Phys. Rev.* **C29** 673 (1984)
[9] J Aichelin and G Bertsch *Phys. Rev.* **C31** 1730 (1985)
[10] A Vicentini, G Jacucci and V R Pandharipande *Phys. Rev.* **C31** 1783 (1985)
[11] D H E Cross *Rep. Prog. Phys.* **53** 605 (1990)
[12] L G Moretto et al. *Phys. Rev. Lett.* **74** 1530 (1995)
[13] T Maruyama et al. *Prog. Theor. Phys.* **87** 1367 (1992)
[14] K Niita et al. *Phys. Rev.* **C52** 2620 (1995)
[15] G Agakishiev et al. [HADES Collaboration] *Eur. Phys. J.* **A40** 45 (2009)
[16] Ž Todorović, S Savović and A Djordjevich *Radiat. Meas.* **43** 179 (2008)
[17] T Aaltonen et al. [CDF collaboration] *Phys. Rev.* **D80** 052003 (2009)
[18] F D Aaron et al. [H1 and ZEUS Collaboration] *JHEP* **1003** 035 (2010)
[19] V Khachatryan et al. [CMS Collaboration] *Phys. Rev. Lett.* **105** 022002 (2010)
[20] K Aamodt et al. [ALICE Collaboration] *Eur. Phys. J.* **C68** 89 (2010)
[21] G Aad et al. [ATLAS Collaboration] *Phys. Lett.* **B694** 327 (2011)
[22] R Aaij et al. [LHCb Collaboration] *Phys. Lett.* **B694** 209 (2010)
[23] J M Feng, C X Tian, R F Si and F H Liu *J. Korean Phys. Soc.* **61** 518 (2012)
[24] J M Feng, *Master Degree Thesis*, (Shanxi University, China) (2012)
[25] F H Liu et al. *Int. J. Mod. Phys.* **E12** 713 (2003)
[26] F H Liu, N N Abd-Allah and B K Singh *Phys. Rev.* **C69** 057601 (2004)
[27] F H Liu *Nucl. Phys.* **A810** 159 (2008)
[28] F H Liu and J S Li *Phys. Rev.* **C78** 044602 (2008)
[29] F H Liu et al. *Chin. J. Phys.* **49** 601 (2011)
[30] Q W Lü, L L Liu, F H Liu and N N Abd-Allah *J. Korean Phys. Soc.* **59** 2684 (2011)
[31] G Agakichiev et al. [HADES collboration] *Eur. Phys. J.* **A41** 243 (2009)
[32] F Abe et al. *Nucl. Instrum. Methods***A271** 387 (1988)
[33] D Acosta et al. [CDF Collaboration] *Phys. Rev.* **D71** 052003 (2005)
[34] A Abulencia et al. [CDF Collaboration] *J. Phys.* **G34** 2457 (2007)
[35] T Aaltonen et al. [CDF Collaboration] *Phys. Rev.* **D77** 112001 (2008)
[36] F D Aaron et al. [H1 Collaboration] *Eur. Phys. J.* **C64** 251 (2009)
[37] S Chekanov et al. [ZEUS Collaboration] *Phys. Lett.* **B672** 106 (2009)
[38] G I Veres for the PHOBOS Collaboration *Indian J. Phys.* **85** 1015 (2011)
[39] L Stiles and M Murray for the BRAHMS Collaboration *Indian J. Phys.* **85** 1039 (2011)
[40] M Spousta for the ATLAS Collaboration *Indian J. Phys.* **85** 1063 (2011)
[41] Y Ming for the STAR Collaboration *Indian J. Phys.* **85** 861 (2011)
[42] H Liu and M Liu for the PHENIX Collaboration *Indian J. Phys.* **85** 803 (2011)
[43] M K Singh, A K Soma, R Pathak and V Singh *Indian J. Phys.* **85** 1523 (2011)
[44] J X Sun, L L Liu, E Q Wang and F H Liu *Indian J. Phys.* doi: 10.1007/s12648-012-0193-0 (2012)